Quantitative analysis of the x-ray diffraction intensities of undulated smectic phases in bent-core liquid crystals

C. L. Folcia,[1] J. Ortega,[2] and J. Etxebarria[1]

[1]*Departamento de Física de la Materia Condensada, Facultad de Ciencia y Tecnología, Universidad del País Vasco, Apartado 644, 48080 Bilbao, Spain*

[2]*Departamento de Física Aplicada II, Facultad de Ciencia y Tecnología, Universidad del País Vasco, Apartado 644, 48080 Bilbao, Spain*

(Received 18 January 2007; published 25 July 2007)

X-ray diffraction diagrams of undulated smectic phases in bent-core liquid crystals have been theoretically studied. The intensities of the reflections have been obtained for different layer modulations, and a general expression has been deduced for orthogonal cells in terms of the different harmonics of the distortion. The case of sinusoidal modulation is especially simple and has been studied also in oblique cells. High-quality x-ray measurements of three compounds reported in the literature have been analyzed as examples. In all cases it has been deduced that the modulation is sinusoidal and its amplitude has been easily obtained by fitting the experimental intensities. Equatorial ($h0$) reflections have been also considered to obtain information about the structure of defects at the maxima and minima of the undulation.

DOI: 10.1103/PhysRevE.76.011713 PACS number(s): 61.30.−v, 61.30.Cz, 61.10.Eq

I. INTRODUCTION

Bent-core liquid crystals [1–3] present a great variety of new mesophases that exhibit interesting phenomena such as spontaneous desymmetrization, ferroelectricity, and nonlinear optical properties. However, the structure of the different mesophases and its origin are not fully understood in many cases. For this reason, they have attracted great attention among the scientific community and many efforts have been made to clarify these points. One of the most powerful experimental techniques to determine the structure of the mesophases is x-ray diffraction. By using this technique it has been observed that very often bent-core mesophases present two-dimensional periodicity. However, in these cases, the structures are especially complex and some of them have not been clarified up to now. In fact, in many works just a basic indexing of the reflections has been reported. In other words, only the peak positions are used to extract structural data, whereas the piece of information contained in the intensities of the reflections is not considered. As a consequence, scarce examples of elaborated structural determinations have appeared in the literature [4–18].

Among the two-dimensional periodic mesophases the case of the undulated smectic phases (USmCP), also named $B7$ phases, is especially interesting. Their x-ray diffraction patterns present a set of commensurate reflections, indicating a layered structure, with a group of incommensurate satellites attached to the main reflections [10,14,19–21]. The first full structural determination of this kind of phases was carried out in the so-called MHOBOW compound by Coleman *et al.* [10], who observed the undulation of the smectic layers by means of transmission electron microscopy on freeze fracture sections. Here MHOBOW stands for the racemic mixture of 1,3 benzene [4-(4 nonyloxyphenyliminomethyl) benzoate] {4′ [4(1-methylhepthyloxycarbonyl) phenyliminomethyl]benzoate}. Evidence of undulated layers allowed these authors to perform a quantitative interpretation of the x-ray diagram obtained with synchrotron radiation on powder samples. The diffraction pattern was indexed on the basis of a rectangular lattice and, in addition, the peak intensities were also considered to obtain the amplitude of a sinusoidal layer modulation compatible with them. However, the fitting procedure was rather tedious, implying the computation of several Taylor's expansions with many terms (up to 19 [11]). As a whole, the method is so cumbersome that it has been never repeated again for any other compound.

In this work we show that the x-ray diffraction pattern of USmCP phases can be analyzed quantitatively in a much simpler way. First, in Sec. II, we present the basics of the diffraction diagrams of two-dimensional liquid crystal phases in order to obtain the general expression of the structure factor and introduce the notation. Next, the diffraction pattern of a rectangular USmCP structure is described in the case of a general nonharmonic layer modulation. The case of sinusoidal modulation is especially treated due to its simplicity and importance. The theoretical model is finally extended to the case of sinusoidally modulated structures with oblique translation lattices. As an illustration, in Sec. III we analyze quantitatively some real x-ray powder patterns of three different materials with USmCP phases reported in the literature [10,20,21]. The shape and amplitude of the modulations are easily determined.

II. DIFFRACTION DIAGRAM OF TWO-DIMENSIONAL LIQUID CRYSTAL PHASES

A. General case

Regarding the small-angle region of a nonresonant x-ray diffraction pattern, an undulated or a columnar liquid crystal phase is an electron density $\rho(\boldsymbol{R})$ with the following characteristics: It presents a periodicity defined by a translation lattice $\boldsymbol{T}=m\boldsymbol{a}+n\boldsymbol{c}$, with m and n integers (see Fig. 1), and a continuous translation symmetry along a direction perpendicular to $\boldsymbol{a}$ and $\boldsymbol{c}$ ($\boldsymbol{b}$ in Fig. 1). This continuous symmetry is due to the fact that the molecules are distributed in a liquid disorder fashion along this direction. Accordingly $\rho(\boldsymbol{R})$ may be expressed in the form

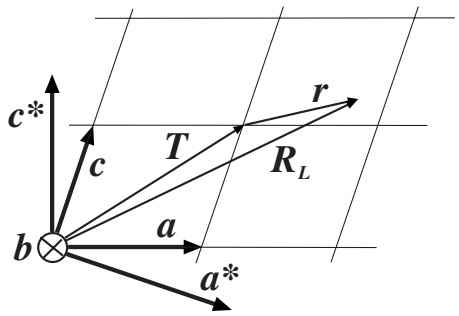

FIG. 1. Schematic representation of a two-dimensional translation lattice together with its reciprocal vectors.

$$\rho(\boldsymbol{R}) = \sum_{\boldsymbol{T}} \rho_0(\boldsymbol{R}_L - \boldsymbol{T}). \tag{1}$$

ρ_0 in Eq. (1) is the motif that is repeated through the translation lattice and will be the basis on which different structural models will be analyzed. The symmetry of ρ_0 is given by one of the 17 plane groups and is obtained from the special projection of the layer group of the real three-dimensional (3D) structure on the $(\boldsymbol{a},\boldsymbol{c})$ plane. We have also defined $\boldsymbol{R}_L$ so that $\boldsymbol{R}=\boldsymbol{R}_L+Y\hat{\boldsymbol{b}}$. Here Y is a continuous variable.

For nonresonant scattering, the diffraction amplitude $G(\boldsymbol{S})$ is the Fourier transform of the electron density $\rho(\boldsymbol{R})$. The diffraction vector $\boldsymbol{S}$ is defined as $\boldsymbol{S}=\boldsymbol{Q}/2\pi$, $\boldsymbol{Q}$ being the scattering wave vector. We have therefore

$$\begin{aligned} G(\boldsymbol{S}) &= \int \left[\sum_{\boldsymbol{T}} \rho_0(\boldsymbol{R}_L - \boldsymbol{T})\right] e^{2\pi i \boldsymbol{S}\cdot\boldsymbol{R}} d^3\boldsymbol{R} \\ &= \int_{-\infty}^{\infty} e^{2\pi i S_Y Y} dY \int \left[\sum_{\boldsymbol{T}} \rho_0(\boldsymbol{R}_L - \boldsymbol{T})\right] e^{2\pi i \boldsymbol{S}\cdot\boldsymbol{R}_L} d^2\boldsymbol{R}_L \\ &= \delta(S_Y)\left[\frac{1}{B}\sum_{\boldsymbol{r}^*} \delta(\boldsymbol{S}-\boldsymbol{r}^*)\right] \int \rho_0(\boldsymbol{r}) e^{2\pi i \boldsymbol{S}\cdot\boldsymbol{r}} d^2\boldsymbol{r}, \end{aligned}$$

B being the cell area and $S_Y=\boldsymbol{S}\cdot\hat{\boldsymbol{b}}$. The Dirac delta function $\delta(S_Y)=\int_{-\infty}^{\infty} e^{2\pi i S_Y Y} dY$ means that the diffraction diagram is restricted to a plane perpendicular to $\hat{\boldsymbol{b}}$. On the other hand, we have introduced the new variable $\boldsymbol{r}=\boldsymbol{R}_L-\boldsymbol{T}=x\frac{\boldsymbol{a}}{a}+z\frac{\boldsymbol{c}}{c}$ obtaining the diffraction condition $\Sigma_{\boldsymbol{T}} e^{2\pi i \boldsymbol{S}\cdot\boldsymbol{T}} = \frac{1}{B}\Sigma_{\boldsymbol{r}^*}\delta(\boldsymbol{S}-\boldsymbol{r}^*)$, where $\boldsymbol{r}^*=h\boldsymbol{a}^*+l\boldsymbol{c}^*$ is a reciprocal lattice vector.

The intensity of a reflection with diffraction vector $\boldsymbol{S}=h\boldsymbol{a}^*+l\boldsymbol{c}^*$ is given by the squared modulus of the structure factor $F(\boldsymbol{S})$, defined from the expression of $G(\boldsymbol{S})$ as

$$F(\boldsymbol{S}) = \frac{\delta(S_Y)}{B} \int \rho_0(\boldsymbol{r}) e^{2\pi i \boldsymbol{S}\cdot\boldsymbol{r}} d^2\boldsymbol{r},$$

so that, leaving aside the Dirac delta function, we have for the (hl) reflection

$$F(hl) = \frac{1}{B} \int \rho_0(x,z) e^{2\pi i (hx/a + lz/c)} dx\, dz. \tag{2}$$

$F(hl)$ is a complex quantity that depends on the origin chosen for the unit cell. However, $F(hl)$ becomes real when the cell origin is chosen in such a way that $\rho_0(x,z)=\rho_0(-x,-z)$. This condition for ρ_0 can be achieved for the great majority of mesophases. It is also to be pointed out that the restriction of the diffraction diagram to the $(\boldsymbol{a}^*\boldsymbol{c}^*)$ reciprocal plane means, according to Eq. (2), that only the projection of the molecules on this plane contributes to the observed intensities. As a consequence, the diffraction diagram does not provide information concerning some important aspects of the structure, like the chirality or polarity direction of the molecules, when it is perpendicular to the translation lattice.

One of our objectives is to perform a calculation of $F(hl)$ for different structural models in order to predict the characteristics of the experimental x-ray diffraction diagram. However, it must be noticed that the experimental integrated intensities are generally affected by different factors. For example, apart from effects like polarization factors, absorption, or thermal diffuse scattering, which are nearly constant in the small-angle region, the intensities measured in a powder x-ray diagram contain the multiplicity factor m [number of (hl) reflections with the same Bragg angle] and also the Lorentz factor

$$L = 1/(\sin\theta_B \sin 2\theta_B), \tag{3}$$

which is very important for the smallest angle reflections. θ_B in Eq. (3) is the Bragg angle. The factor of $\sin 2\theta_B$ in Eq. (3) accounts for a simple geometrical consideration: For a given reflection (hl), the power diffracted by the sample is scattered on a cone surface of angle $2\theta_B$. Thus, since the detector captures a given length of the cone circumference, the detected power increases as the perimeter of this circumference decreases—i.e., as the Bragg angle becomes smaller. On the other hand, the $\sin\theta_B$ factor takes into account the proportion of crystals contributing to a given reflection. In summary, once the background intensity has been subtracted, the different integrated intensities obtained from a powder diagram must be divided by m and L in order to check the reliability of a given structural model.

B. USmCP phase

1. Rectangular translation lattice

The existence of harmonically undulated layers in some structures was proposed by Coleman *et al.* [10] to account for the x-ray diffraction diagram observed on two materials that present the so-called $B7$ phase. In that work a mechanism was proposed for the origin of the layers undulation based on the existence of splay of the molecular dipole moments. Here we present a calculation for the diffracted intensities that results in a simple analytical expression. This will be useful for the determination of different structural parameters and allows an easy generalization of the model to nonharmonic layer undulations.

The primitive cell of the undulated smectic structure is represented in Fig. 2 together with its symmetry elements for

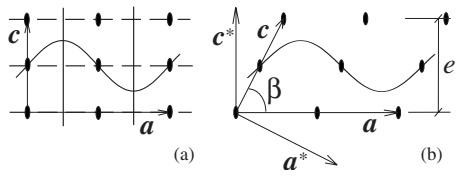

FIG. 2. Primitive cell of a USmCP structure with rectangular (a) and oblique (b) translation lattice. The undulated line represents the center of a smectic layer. In both cases the symmetry elements are indicated. The plane group of the electronic density is $pm2g$ and $p2$ for (a) and (b), respectively. The reciprocal vectors of the oblique lattice are also shown.

the case of rectangular and oblique translation lattice. For the rectangular lattice, the electronic density is

$$\rho_0(x,z) = \rho_0\left(z - \frac{c}{2} - A\,\sin 2\pi\frac{x}{a}\right), \tag{4}$$

where A is the undulation amplitude. If there were no undulation ($A=0$), the electronic density ρ_0 would depend on z as smectic layers usually do. We calculate the structure factor replacing $\rho_0(x,z)$ given by Eq. (4) in expression (2):

$$F(h,l) = \frac{1}{B}\int_0^a e^{2\pi ihx/a}dx \int_{-\infty}^{\infty} \rho_0\left[z - \frac{c}{2} - A\,\sin 2\pi\frac{x}{a}\right] e^{2\pi ilz/c}dz.$$

Now, after introducing the new variable $z' = z - \frac{c}{2} - A\,\sin 2\pi\frac{x}{a}$, it results in

$$F(hl) = \frac{1}{B}e^{i\pi l}f_0(l)\int_0^a e^{2\pi ihx/a}e^{2\pi il(A/c)\sin 2\pi x/a}dx, \tag{5}$$

where $f_0(l)$ may be defined as a kind of form factor for the smectic layer:

$$f_0(l) = \int_{-\infty}^{\infty} \rho_0(z')e^{2\pi ilz'/c}dz'. \tag{6}$$

In order to evaluate the integral on the right-hand-side of Eq. (5) we introduce the Jacobi-Auger identity

$$e^{ix\,\sin\,\theta} = \sum_{m=-\infty}^{\infty} J_m(x)e^{im\theta},$$

$J_m(x)$ being the Bessel function of m order of the first kind. In our case, it results in

$$e^{2\pi il(A/c)\sin 2\pi x/a} = \sum_{m=-\infty}^{\infty} J_m\left(2\pi l\frac{A}{c}\right)e^{im2\pi x/a}.$$

The structure factor is then expressed as follows:

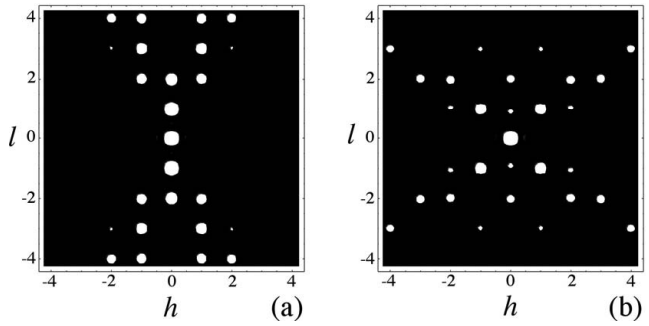

FIG. 3. Small-angle diffraction diagrams calculated from expression (8) for A/c ratios of 0.1 (a) and 0.3 (b). The spot sizes are proportional to the reflection intensities, and only the strongest reflections are shown. $|f_0(l)|$ is assumed to be independent of l in both cases. There are no reflections at the $(h0)$ line.

$$F(hl) = \frac{1}{B}e^{i\pi l}f_0(l)\sum_{m=-\infty}^{\infty} J_m\left(2\pi l\frac{A}{c}\right)\int_0^a e^{2\pi i(x/a)(h+m)}dx$$
$$= \frac{1}{B}e^{i\pi l}f_0(l)\sum_{m=-\infty}^{\infty} J_m\left(2\pi l\frac{A}{c}\right)\left[ae^{i\pi(h+m)}\frac{\sin\,\pi(h+m)}{\pi(h+m)}\right]. \tag{7}$$

Expression (7) is zero unless $h+m=0$—i.e., $m=-h$—in which case it results in

$$F(hl) = \frac{1}{c}e^{i\pi l}f_0(l)J_{-h}\left(2\pi l\frac{A}{c}\right),$$

where it was taken into account that the cell area is $B=ac$. The intensity of the reflection (hl) is therefore

$$I(hl) = \frac{1}{c^2}|f_0(l)|^2\left|J_{-h}\left(2\pi l\frac{A}{c}\right)\right|^2. \tag{8}$$

The simplicity of expression (8) permits an immediate visualization of some general trends of the diffraction diagram that an undulated smectic phase should present. In this respect, Fig. 3 shows a schematic representation of the diffraction diagram as predicted by expression (8) for two different values of the ratio A/c. In order to appreciate the characteristics of the diagram for increasing l, $|f_0(l)|$ was considered independent of l in all cases, though in practice $|f_0(l)|$ is a decreasing function of l. The pattern obviously converges to the one corresponding to a normal smectic phase [where only $(0l)$ reflections are present] as the undulation amplitude decreases.

Our calculation allows an easy generalization of the model to arbitrary undulations $u(x)$ if they are expanded as a linear combination of sinusoidal functions:

$$u(x) = \sum_{k=1}^{N} A_k\,\sin 2\pi k\frac{x}{a}.$$

In this case, after a completely analogous procedure to that explained above, the following expression for the intensity of the (hl) reflection results:

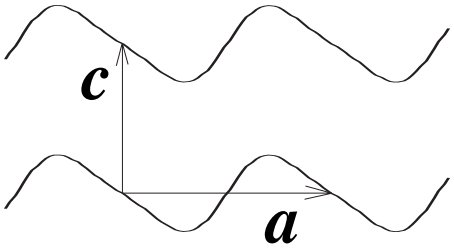

FIG. 4. Scheme of the undulated-smectic structure represented by expression (10). The rectangular lattice parameters $\boldsymbol{a}$ and $\boldsymbol{c}$ are indicated. The plane group of the electron density is $p2$.

$$I(hl) = \frac{1}{c^2}|f_0(l)|^2 \left| \sum_{m_2=-\infty}^{\infty} \sum_{m_3=-\infty}^{\infty} \cdots \sum_{m_N=-\infty}^{\infty} J_{-h-\Sigma_{k=2}^{N} k m_k}\left(2\pi l \frac{A_1}{c}\right) \times \prod_{k=2}^{N} J_{m_k}\left(2\pi l \frac{A_k}{c}\right) \right|^2 . \quad (9)$$

Evidently, in order to perform a quantitative interpretation of the experiment, the number of harmonics must be as small as possible to simplify the expression of $I(hl)$ and reduce the number of the unknown parameters A_k. Let us, for example, consider the case of an electron density modulated as shown in Fig. 4. This represents a monoclinic structure with a rectangular translation lattice, similar to that proposed by Keith *et al.* [22] for undulated synclinic structures. It was just constructed with two harmonics:

$$u(x) = A\left[\sin 2\pi \frac{x}{a} + \frac{1}{5}\sin 2\pi \frac{2x}{a}\right]. \quad (10)$$

Then, the diffracted intensity as obtained from Eq. (9) results:

$$I(hl) = \frac{1}{c^2}|f_0(l)|^2 \left| \sum_{m_2=-\infty}^{\infty} J_{-h-2m_2}\left(2\pi l \frac{A}{c}\right) J_{m_2}\left(2\pi l \frac{A}{5c}\right) \right|^2 , \quad (11)$$

where only a few terms in the sum are enough to achieve a very acceptable convergence. The diffraction diagram predicted by Eq. (11), with constant $|f_0(l)|$, is represented in Fig. 5 for two different values of the ratio A/c.

The usefulness of theoretical diffraction patterns like those of Figs. 3 and 5 is evident when measurements are performed on oriented samples. In those cases the complete reciprocal lattice is obtained at once with a two-dimensional detector, and a qualitative comparison should be enough to establish some general features of the structure like its symmetry (orthorhombic or monoclinic) or the approximate amplitude of the modulation. In addition, it can be expected that expressions like Eqs. (8) and (9) would allow a relatively easy quantitative interpretation of the experimental data. In principle, the standard procedure to account for the experimental x-ray pattern would be as follows: $u(x)$ is first proposed. This could be, for example, a harmonic function or something more general. The layer distortion $u(x)$ should be proposed on the basis of previous experimental results as

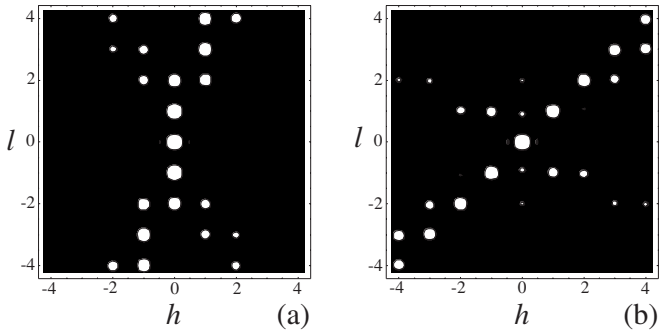

FIG. 5. Small-angle diffraction diagrams calculated from expression (11) for $|f_0(l)|$ independent of l and A/c ratios of 0.1 (a) and 0.3 (b). The sum over m_2 in Eq. (11) is considered to run from −6 to 6, although no variations, even for the weakest reflections, result for $|m_2| \geq 4$. As in Fig. 3, the spot sizes are proportional to the reflection intensities, and only the strongest reflections are shown. There are no reflections at the $(h0)$ line.

well as a qualitative comparison with the obtained x-ray pattern. Then, the relative intensities $I(hl)$ for fixed values of l are fitted to Eq. (8) or (9), taking the ratios A_k/c as parameters.

As can be noticed in Figs. 3 and 5, there are no reflections at the equator of the diffraction diagram—i.e., at the line $(h0)$. Even when this fact is obvious from Eqs. (8) and (9) as $J_m(0)=0$, it occurs whenever the electronic density is of the form $\rho(x,z)=\rho[z-u(x)]$ for arbitrary $u(x)$ since

$$F(h0) = \frac{1}{B}\int \rho_0[z-u(x)]e^{2\pi i(h/a)x}dxdz = \frac{1}{B}\int_0^a e^{2\pi i(h/a)x}dx \int_{-\infty}^{\infty} \rho_0(z')dz' = \frac{1}{c}f_0(0)e^{\pi i h}\frac{\sin \pi h}{\pi h} = 0 \quad (12)$$

unless $h=0$.

We finish this part with one comment about the existence in different materials of the $(h0)$ reflections. Since these reflections are not allowed by virtue of Eq. (12), their existence must be explained by assuming that the undulation is perturbed by the presence of regions where the charge density is somewhat different from ρ_0. According to Coleman *et al.* [10], these regions would be directly related to defect lines that separate areas with splayed polarizations and, as a consequence, defects are formed at the tops and valleys of the undulation. Furthermore, since experimentally there are no restrictions on h for these reflections, defects at the tops and valleys must be different. If they were equal, only $h=2n$ reflections would be observed because the lattice of defects appears centered for any $h\boldsymbol{a}^*$ vector. Anyway, even when these defects make some contribution to the whole diffraction pattern, it is important to point out that the observed $(h0)$ reflections occur at very small angles and, therefore, are greatly enhanced by the Lorentz factor. Thus, their structure factors have amplitudes much smaller than any other in the pattern and, consequently, it can be assumed that expressions like Eqs. (8) and (9), where the existence of defects is not

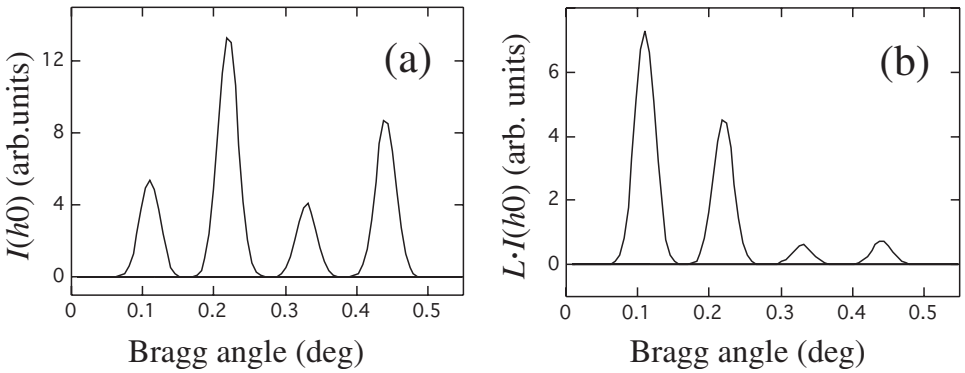

FIG. 6. (a) ($h0$) Bragg peaks calculated from expression (13) considering $f_d^v=0.25f_d^p$ and $d=0.1a$ for a lattice parameter $a=400$ Å. A Gaussian profile with constant width is assumed for all the reflections. (b) A simulation of the experimentally observed peaks is performed by multiplying the peak intensities in (a) by the Lorentz factor L [expression (3)].

considered, constitute valid predictions for the measured intensities of the diffraction diagram. Figure 6(a) represents the ($h0$) intensities calculated by modeling the defects as constant charge densities ρ_d^p and ρ_d^v located at the peaks and valleys, respectively, extending each one a length d. From the general expression (2), the intensities result:

$$I(h0)=\left|\frac{1}{ac}\frac{\sin\left(\pi h\frac{d}{a}\right)}{\pi\frac{h}{a}}[f_d^p(0)+e^{\pi ih}f_d^v(0)]\right|^2, \quad (13)$$

where $f_d^{p,v}(0)=\int_{-\infty}^{\infty}\rho_d^{p,v}(z)dz$ is the form factor of the defects. The effect of the Lorentz factor on the peaks intensities is shown in Fig. 6(b). In this case, a lattice parameter $a=400$ Å, typical for $B7$ phases, was selected. As can be seen, the height of the peaks decreases as h increases. This is just the behavior experimentally observed [10,20,21].

2. Oblique translation lattice

For the sake of completeness, we extend the above calculation to the case of a sinusoidal structure with an oblique translation lattice [see Fig. 2(b)]. The electron density is now

$$\rho_0(x,z)=\rho_0\left[z-\frac{e}{2}-A\sin\frac{2\pi}{a}\left(x-\xi\frac{e}{2}\right)\right],$$

where $\xi=\cot\beta$. It is convenient to express the translation and reciprocal vectors in the x, z coordinate frame:

$$\boldsymbol{a}=a\hat{\boldsymbol{x}}, \quad \boldsymbol{a}^*=\frac{1}{a}\hat{\boldsymbol{x}}-\frac{\xi}{a}\hat{\boldsymbol{z}}, \quad (14)$$

$$\boldsymbol{c}=\xi e\hat{\boldsymbol{x}}+e\hat{\boldsymbol{z}}, \quad \boldsymbol{c}^*=\frac{1}{e}\hat{\boldsymbol{z}}, \quad (15)$$

in order to express the structure factor in the form

$$F(\boldsymbol{S})=\frac{1}{B}\int\rho_0(\boldsymbol{r})e^{2\pi i\boldsymbol{S}\cdot\boldsymbol{r}}d^2\boldsymbol{r}$$

$$=\frac{1}{ac\sin\beta}\int\rho_0(x,z)e^{2\pi i(S_xx+S_zz)}\,dx\,dz\sin\beta.$$

According to Eqs. (14) and (15), $S_x=h\frac{1}{a}$ and $S_z=l\frac{1}{e}-h\frac{\xi}{a}$. The intensity of the ($hl$) reflection results:

$$I(h,l)=\frac{1}{c^2}|f_0(h,l)|^2\left|J_{-h}\left[2\pi\left(\frac{l}{e}-h\frac{\xi}{a}\right)A\right]\right|^2, \quad (16)$$

where the smectic layer form factor is

$$f_0(h,l)=\int_{-\infty}^{\infty}\rho_0(z')e^{2\pi i(l/e-h\xi/a)z'}dz',$$

i.e., depends on h and l and, therefore, an easy quantitative comparison of expression (16) with the experimental pattern is not possible as before since there are not lines of reflections where f_0 is constant. In addition, the x-ray diagram is indexed on the basis of a primitive oblique lattice, and there are reflections also in the ($h0$) line, even without considering defects. The intensities of the ($h0$) reflections vanish as the oblique angle β tends to $\pi/2$.

III. ILLUSTRATIVE EXAMPLES WITH REAL STRUCTURES

Now we turn to apply the procedure described above to the structural determination of several USmCP phases. Although a relatively large number of materials are supposed to present this kind of structures, not many have been measured with the required accuracy. In order to use the intensity data, clearly resolved peaks are necessary. In addition, it is interesting to have as many reflections as possible. Therefore, highly monochromatic and intense sources of x-ray radiation (synchrotron) should inevitably be used in the experiments. We will restrict ourselves to analyze just three compounds for which such high quality measurements exist. (hl) reflections with at least $l=0$, 1, and 2 are satisfactorily characterized in those experiments. The materials are the already quoted MHOBOW [10], 1,3-phenylene bis [4-(3-chloro-4-octyloxyphenyliminomethyl)bezoate] (PBCOB) [10,20], and 1,3-phenylene bis{4-[3-fluoro-4-(3(S),7-dimethyloctyloxy)-phenyliminomethyl]benzoate} (PBFDOB) [21].

The general aspect of a typical powder x-ray diffractogram is schematized in Fig. 7, where the data for PBFDOB are presented. The indexation of the peaks indicated in the figure has been carried out using an orthogonal cell. Qualitatively similar diffraction patterns are obtained for MHOBOW and PBCOB.

Table I gathers the different structural parameters for the three compounds, and in Fig. 8 we compare the observed and calculated intensities for the $l=0$, 1, and 2 reflections. Peaks

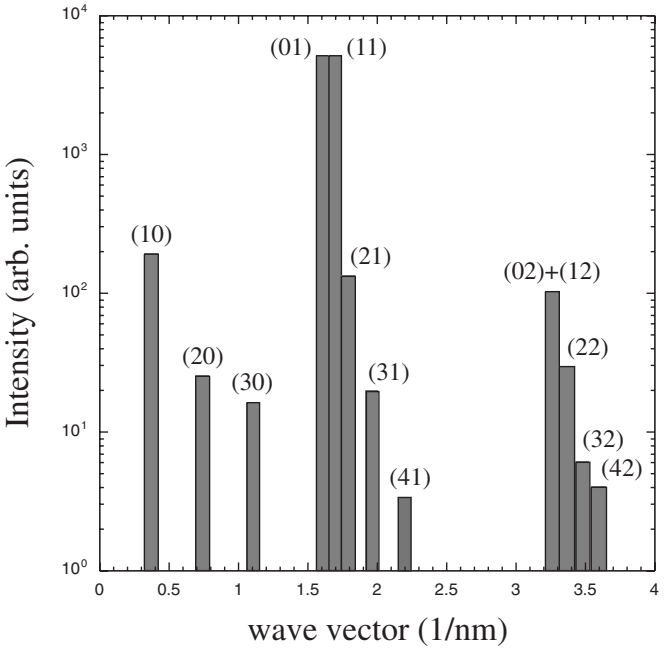

FIG. 7. Schematic representation of the powder diffraction diagram obtained by Lee *et al.* for the material PBFDOB using synchrotron radiation [see Fig. 6(b) of Ref. [21]]. Each bar represents an observed peak. Its height is proportional to the integrated intensity extracted from the experimental pattern after background subtraction. The diffraction diagram is indexed on the basis of a rectangular lattice, obtaining the set of Miller indices that appear in the figure. Only peaks with $l=0$, 1, and 2 are considered.

with $l=3$ or larger are too small to be used. For $l=1$ and 2, the intensities were computed using Eq. (8), so that a simple sinusoidal modulation was assumed. As can be seen the accordance is rather good, which means that this model is a rather good approach to describe the layer distortion. In order to fit the modulation amplitude A the following expression has been minimized:

$$\sum_{l,h} \frac{\left[I_{\text{expt}}(h,l) - C_l J_{-h}^2\left(2\pi l \frac{A}{c}\right)\right]^2}{I_{\text{expt}}(h,l)}, \tag{17}$$

where the indices h and l run over positive and negative values. As we have used powder diffraction data and the cell is orthogonal, each $I_{\text{expt}}(h,l)$ is obtained from the corresponding experimental peak intensity with positive indices divided by its multiplicity and the Lorentz factor. C_l is a fitting scale factor corresponding to each set of l reflections. Obviously $C_l=C_{-l}$, and $I_{\text{expt}}(h,l)$ appearing in the denominator stands for the squared standard deviation σ^2 corresponding to a Poisson distribution. In the case of MHOBOW the A value deduced from our fit (see Table I) is in good agreement with that obtained before [10] using a more complicated method.

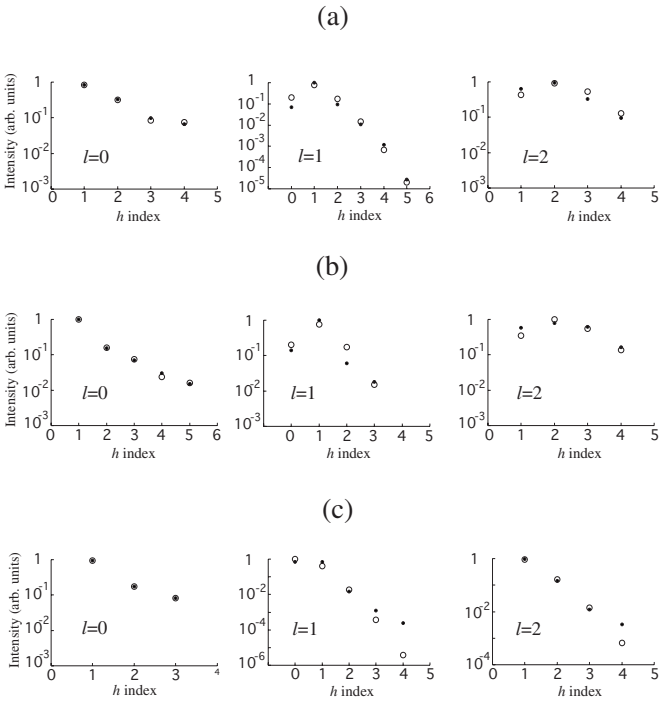

FIG. 8. Experimental (solid circles) and fitted (open circles) integrated intensities of the studied compounds: (a) MHOBOW, (b) PBCOB, and (c) PBFDOB. Ordinate axes indicate the intensity in arbitrary units in all the cases. For the fitting, a sinusoidal modulation is assumed in the three compounds. Peak intensities corresponding to $l=0$ are fitted to expression (13). Apart from an arbitrary scale factor, two different parameters are obtained for each compound. The resulting d and X parameters appear in Table I. The modulation amplitude A is obtained by minimizing expression (17) using the peak intensities for $l=1$ and $l=2$. The obtained amplitudes are compiled in Table I. In the three cases, the (02) and (12) reflections are overlapped in the experimental diagrams. Thus, given the multiplicity of these reflections ($m=2$ and $m=4$, respectively), the observed intensities are fitted to $2I(02)+4I(12)$.

In Fig. 8 the data for the $(h0)$ reflections are also presented. In this case, the intensities were computed using Eq. (13) after taking into account the Lorentz factor correction. Also, here, good accordance is found between theory and

TABLE I. Structural parameters of the materials analyzed in the present study. The undulation amplitude A is obtained from the fit of the experimental intensities to expression (8). Similarly, the defect parameters d and X are evaluated according to expression (13) using the $(h0)$ reflections.

Compound	a (Å)	c (Å)	A (Å)	d (Å)	X
MHOBOW	274	39.5	10.7	12.6	0.13
PBCOB	279	38.6	10.0	26.8	−0.09
PBFDOB	170	38.5	5.0	18.7	−0.04

experiment. The parameters deduced from the fits are d/a (the length of the defect relative to the a lattice parameter) and X, the ratio between the form factors of the defects at the peaks and at the valleys (or vice versa). As can be seen in Table I both d/a and X are in all cases about 0.1. This means on the one hand that the region where the defects are concentrated is only a small percentage of the whole smectic layer area (as it should be if we can properly speak of defects). On the other hand, the small X value suggests that the deviation from the defect-free electron density is essentially accumulated either at the peaks or at valleys, but not at both positions simultaneously. This is compatible with the idea previously pointed out in Ref. [10] that the electron density is not the same at the peaks and at the valleys. Additionally to this idea, we have found that the principal defects are mainly located either at the minima or maxima of the undulation. At the opposite position, the importance of the defect is much smaller.

IV. CONCLUSIONS

We have investigated the x-ray diffraction diagram of USmCP phases in bent-core materials. For sinusoidal modulations very simple expressions are obtained for the intensity of the x-ray reflections. The theoretical analysis has been extended to more general situations, including modulations containing several harmonics or oblique cells. We have presented some examples of application studying three compounds for which high-quality x-ray measurements already existed in the literature. In all cases the amplitudes of the modulation have been deduced from very simple fits of the experimental intensities. From the analysis of the intensities of $(h0)$ reflections we have obtained information about the structure of defects that are formed at the minima and maxima of the undulation.

ACKNOWLEDGMENTS

This work was supported by Project Nos. MAT2003-07806-C02-02 and MAT2006-13571-C02-02 (CICYT-FEDER) from Spain-EU and by the University of the Basque Country (Project No. 9/UPV 00060.310-13562/2001).

[1] G. Pelzl, S. Diele, and W. Weissflog, Adv. Mater. (Weinheim, Ger.) **11**, 707 (1999).
[2] R. A. Reddy and C. Tschierske, J. Mater. Chem. **16**, 907 (2006).
[3] H. Takezoe and Y. Takanishi, Jpn. J. Appl. Phys., Part 1 **45**, 597 (2006).
[4] Y. Takanishi, T. Izumi, J. Watanabe, K. Ishikawa, H. Takezoe, and A. Iida, J. Mater. Chem. **9**, 2771 (1999).
[5] J. Szydlowska, J. Mieczkowski, J. Matraszek, D. W. Bruce, E. Gorecka, D. Pociecha, and D. Guillon, Phys. Rev. E **67**, 031702 (2003).
[6] K. Pelz, W. Weissflog, U. Baumeister, and S. Diele, Liq. Cryst. **30**, 1151 (2003).
[7] R. A. Reddy, B. K. Sadashiva, and V. A. Raghunathan, Chem. Mater. **16**, 4050 (2004).
[8] R. A. Reddy, V. A. Raghunathan, and B. K. Sadashiva, Chem. Mater. **17**, 274 (2005).
[9] R. A. Reddy, U. Baumeister, C. Keith, and C. Tschierske, J. Mater. Chem. **17**, 62 (2007).
[10] D. A. Coleman, J. Fernsler, N. Chattham, M. Nakata, Y. Takanishi, E. Körblova, D. R. Link, R. F. Shao, W. G. Jang, J. E. Maclennan, O. Mondainn-Mova, C. Boyer, W. Weissflog, G. Pelzl, L. C. Chien, J. Zasadzinski, J. Watanabe, D. M. Walba, H. Takezoe, and N. Clark, Science **301**, 1204 (2003).
[11] D. A. Coleman, Ph.D. thesis, University of Colorado, 2003.
[12] E. Gorecka, D. Pociecha, J. Mieczkowski, J. Matraszek, D. Guillon, and B. Donnio, J. Am. Chem. Soc. **126**, 15946 (2004).
[13] M. Nakata, D. R. Link, Y. Takanishi, Y. Takahasi, J. Thisayukta, H. Niwano, D. A. Coleman, J. Watanabe, A. Iida, N. A. Clark, and H. Takezoe, Phys. Rev. E **71**, 011705 (2005).
[14] C. Keith, R. A. Reddy, U. Baumeister, and C. Tschierske, J. Am. Chem. Soc. **126**, 14312 (2004).
[15] C. L. Folcia, J. Etxebarria, J. Ortega, and M. B. Ros, Phys. Rev. E **72**, 041709 (2005).
[16] Y. Takanishi, M. Toshimitsu, M. Nakata, N. Takada, T. Izumi, K. Ishikawa, H. Takezoe, J. Watanabe, Y. Takahashi, and A. Iida, Phys. Rev. E **74**, 051703 (2006).
[17] C. L. Folcia, I. Alonso, J. Ortega, J. Etxebarria, I. Pintre, and M. B. Ros, Chem. Mater. **18**, 4617 (2006).
[18] C. L. Folcia, J. Etxebarria, J. Ortega, and M. B. Ros, Phys. Rev. E **74**, 031702 (2006).
[19] G. Pelzl, M. W. Schröder, U. Dunemann, S. Diele, W. Weissflog, C. Jones, D. A. Coleman, N. A. Clark, R. Stannarius, J. Li, B. Das, and S. Grande, J. Mater. Chem. **14**, 2492 (2004).
[20] C. Lee, A. Primak, A. Jákli, E. Choi, W. Zin, and L. Chien, Liq. Cryst. **28**, 1293 (2001).
[21] C. Lee, S. Kwon, T. Kim, E. Choi, S. Shin, W. Zin, D. Kim, J. Kim, and L. Chien, Liq. Cryst. **30**, 1401 (2003).
[22] C. Keith, R. A. Reddy, A. Hauser, U. Baumeister, and C. Tschierske, J. Am. Chem. Soc. **128**, 3051 (2006).